



Grounded running in quails: Simulations indicate benefits of observed fixed aperture angle between legs before touch-down

Emanuel Andrada ^{a,*}, Christian Rode ^{a,b}, Reinhard Blickhan ^a

^a *Science of Motion, Friedrich-Schiller University Jena, Seidelstr. 20, 07749 Jena, Germany*

^b *Locomotion Lab, Technische Universität Darmstadt, Magdalenenstr. 27, 64289 Darmstadt, Germany*



HIGHLIGHTS

- With experiments and simulations we investigated grounded running.
- Quails fixed the angle between legs (aperture angle) before touch-down.
- Aperture angle correlates with dynamical relevant parameters.
- Fixed angle of attack strategy is not feasible for grounded running.
- The fixed aperture angle strategy improved model stability.

ARTICLE INFO

Article history:

Received 10 January 2013

Received in revised form

14 June 2013

Accepted 25 June 2013

Available online 3 July 2013

Keywords:

Avian locomotion

Grounded running

Spring-mass

Biomechanics

Aperture angle

ABSTRACT

Many birds use grounded running (running without aerial phases) in a wide range of speeds. Contrary to walking and running, numerical investigations of this gait based on the BSLIP (bipedal spring loaded inverted pendulum) template are rare. To obtain template related parameters of quails (e.g. leg stiffness) we used x-ray cinematography combined with ground reaction force measurements of quail grounded running. Interestingly, with speed the quails did not adjust the swing leg's angle of attack with respect to the ground but adapted the angle between legs (which we termed aperture angle), and fixed it about 30 ms before touchdown. In simulations with the BSLIP we compared this swing leg alignment policy with the fixed angle of attack with respect to the ground typically used in the literature. We found symmetric periodic grounded running in a simply connected subset comprising one third of the investigated parameter space. The fixed aperture angle strategy revealed improved local stability and surprising tolerance with respect to large perturbations. Starting with the periodic solutions, after step-down step-up or step-up step-down perturbations of 10% leg rest length, in the vast majority of cases the bipedal SLIP could accomplish at least 50 steps to fall. The fixed angle of attack strategy was not feasible. We propose that, in small animals in particular, grounded running may be a common gait that allows highly compliant systems to exploit energy storage without the necessity of quick changes in the locomotor program when facing perturbations.

© 2013 Elsevier Ltd. All rights reserved.

1. Introduction

Gait categories, based on duty factor, do not necessarily correspond to functional categories based on overall leg behaviour or center of mass (CoM) movement (i.e. pendulum-like or spring-like behavior (Cavagna et al., 1976)). In avian terrestrial locomotion, three gaits are frequently observed: walking, grounded running (Hancock et al., 2007; Nudds et al., 2011; Rubenson et al., 2004) (also referred to as compliant walking (Clark and Alexander, 1975)), and running (also referred to as

aerial running (Nudds et al., 2011)). Grounded running combines duty factors traditionally linked to walking (duty factors > 0.5, i.e. double support phases exist) with running-like energy fluctuations of the body, i.e. potential and kinetic energy change nearly in phase (Cavagna 1975; Heglund et al., 1982). While the evolutionary relevance of both walking and running and some of the optimization criteria and constraints imposed by these gaits on the locomotor system are well documented for birds and humans (Hancock et al., 2007; Nudds et al., 2011; Rubenson et al., 2004; Clark and Alexander, 1975; Heglund et al., 1982; Saibene and Minetti, 2003; Minetti et al., 1994; Gatesy and Biewener, 1991; Gatesy and Middleton, 1997; Muir et al., 1996), they are not as clear for grounded running.

For activities such as exploration and foraging birds favor the walking gait. Running allows them to escape from predators, or to

* Corresponding author. Tel.: +49 3641945710.

E-mail addresses: emanuel.andrada@uni-jena.de, eman.andrada@gmail.com (E. Andrada).

Nomenclature

CoM	body center of mass	ϕ_{leg}	aperture angle between legs
CoP	center of pressure	ϕ_{leg0}	aperture angle between legs at touch-down
GRF	ground reaction force	ϕ_v	aperture angle between virtual legs
BW	body weight	ϕ_0	aperture angle between virtual legs at touch-down
SSPh	single support phase	m	body mass
DSPh	double support phase	k	spring stiffness
mp	maximum protraction	g	gravity
tob	tip of beak	l_0	spring rest length
occ	occiput	E	system energy
cmc	caudalmost cervical vertebrae	E_p	potential energy
tomt	tip of middle toe	E_k	kinetic energy
TD	touch down	ω_0	natural frequency of the system
TO	take off	\hat{k}	dimensionless leg stiffness
a, v, s	acceleration, speed and position of the CoM	\hat{l}_0	dimensionless rest length
SLIP	spring loaded inverted pendulum	\hat{x}_{rel}, \hat{y}	system state variables
LTP	lower turning point	\hat{E}	dimensionless system energy
α_{leg}	leg orientation	ψ	leg compression
α	virtual leg orientation	GR	grounded running speed
α_0	angle of attack at touch-down	P	Poincaré map
		DP	linearized Poincaré map
		λ_i	eigenvalues of the linearized Poincaré map

travel long distances economically at higher speeds (Hancock et al., 2007; Nudds et al., 2011; Rubenson et al., 2004; Heglund et al., 1982). It has been hypothesized that grounded running associated with more compliant limbs may facilitate the control of head movements, thereby improving visual stability (Hancock et al., 2007). Transitioning between walking and grounded running has also been associated with a reduction in the metabolic cost of transport in the ostrich (Rubenson et al., 2004). Others have suggested that always keeping at least one foot in contact with the ground provides the ability to perform fast turns, something which in the wild may be more relevant than energy saving or speed (Gatesy and Biewener, 1991; Daley and Usherwood, 2010).

Apart from economic considerations, simulations of walking and running using the bipedal spring-loaded inverted pendulum model (BSLIP) indicate the exploitation of self-stable modes in bipedal locomotion (Seyfarth et al., 2002, 2003; Geyer et al., 2006). Although animals use numerous sensory and neuromuscular mechanisms during movement (e.g. Pearson, 1995; Dietz, 1996), the use of self-stable modes, i.e. tuning parameters like leg stiffness to regions of BSLIP stability, may relax the required neural control in coping with internal or external perturbations during locomotion (Blickhan et al., 2007). For example, BSLIP parameters adopted by humans in running and walking mostly correspond to BSLIP regions of stability (Seyfarth et al., 2002, 2003; Geyer et al., 2006).

Contrary to walking and running (e.g. Seyfarth et al., 2002, 2003; Geyer et al., 2006; Blickhan, 1989), numerical investigations on grounded running are rare. Recently Rummel et al. (2009) reported periodic BSLIP grounded running within a very narrow range of rather slow speeds, steep contact angles and constant high stiffness. It is however not known whether periodic grounded running can be generated by the BSLIP model in the parameter space that birds prefer. Moreover, it is not clear how simple swing leg control strategies might influence the stability of such eventual periodic solutions.

In preliminary experiments we observed that, during grounded running, the angle between legs (which we termed aperture angle) was fixed by the quails in a time period before touchdown. This fixed aperture angle between legs represents a swing leg retraction scheme not reported before. It leads to swing leg retraction related to stance leg rotation. In contrast, in BSLIP

simulations of locomotion the swing leg is typically held at a constant angle with respect to the ground (Seyfarth et al., 2002, 2003; Geyer et al., 2006).

In this paper, we experimentally verify the use of a fixed aperture angle in quail grounded running and numerically analyze possible benefits of this leg alignment strategy compared to the fixed angle of attack. To this end, we estimate BSLIP related dimensionless parameters (e.g. leg stiffness, leg length, angle of attack, aperture angle) using kinematic x-ray motion analysis and single limb force plate measurements during quail grounded running. Within the obtained parameter range we analyze the stability of grounded BSLIP running applying both leg alignment strategies. Finally, we compare and discuss model predictions with experimental findings.

2. Methods

2.1. Experiments

For our investigation of steady grounded running we disregarded trials with (1) the CoP of any leg being outside the force plate area (2) a horizontal speed deviation of more than 5% between the force plates (non-steady state trials); (3) aerial phases; and (4) a phase shift between potential (E_p) and kinetic energy (E_k) above 45° (non-bouncing mechanics) (Ahn et al., 2004). We obtained E_p and E_k as described by Cavagna (1975). Vertical displacements of the body's CoM were used to calculate the changes in E_p , whereas the differentiation of the displacements was used to calculate changes in the CoM's speed and thus the changes of its translational kinetic energy (with horizontal and vertical kinetic components being summed up to total kinetic energy E_k). We then calculated the phase shift between E_p and E_k as the time between absolute minima of E_p and E_k divided by stride time multiplied by 360°.

2.1.1. Animals

We obtained kinematic and kinetic data from four adult quails (*Coturnix coturnix*) weighing between 180 and 240 gr. While two quails voluntarily moved across the track when released, two needed motivation (clapping or lightly tipping the tail) to move across a 3 m long walking-track at their preferred speeds. We covered the track with sand paper to reduce slipping. The

Committee for Animal Research of the State of Thuringia, Germany, approved the animal care and experimental procedures.

2.1.2. X-ray motion analysis

We recorded kinematics using biplanar x-ray cineradiography (Fig. 1A) at the Institut für Spezielle Zoologie und Evolutionsbiologie mit Phyletischem Museum, Germany. Our experimental setup consisted of a biplanar x-ray system (Neurostar, Siemens[®]) and two standard light high-speed cameras (SpeedCam Visario g2, Weinberger[®]). We arranged the x-ray sources to obtain the sagittal and dorso-ventral projections of the moving bird. With this setup, we filmed the animals at 40 kV and 53 mA, with a sampling frequency of 1 kHz. We filtered the raw video data (e.g. gamma correction, contrast, sharpness) and, finally, identified the location of the joints using SimiMotion[®] software.

2.1.3. Force data acquisition

We measured three-dimensional substrate reaction forces and CoP (center of pressure) with two custom-built (8 cm × 9 cm) force plates, which we integrated into the walking-track. In order to reduce metal parts in the area of the x-ray beams, we used carbon fiber to construct the force plates and their support. We used 6-DOF (degree of freedom)

force-torque sensors (ATI nano17[®]) as transducer elements. Using fast Fourier transformation, we measured the plates' natural frequency, which was above 200 Hz. Furthermore, our static tests revealed the resolution of the CoP position to be below 1 mm at loads higher than 300 mN (about 15% of the quail's body weight). According to the sampling rate of the kinematic data, we collected ground reaction forces at 1 kHz (NI USB-6229, National Instruments[®]; custom software LabView 2009 National Instruments[®]). We synchronized force and x-ray analysis electronically (post-trigger).

2.1.4. Experimental parameters

As we will show in Sections 2.2 and 3.2, four dimensionless quantities describe the dynamic similarity of the dimensionless BSLIP: the dimensionless stiffness (\hat{k}), the angle of attack (α_0) or the aperture angle (ϕ_0), the leg compression ψ , and the grounded running speed (GR). To enable comparison of experiments with simulations, we determined these template related parameters from our experiments with quails.

In birds, the CoM is located cranially to the hip, and, therefore, legs and virtual legs differ (Fig. 1B). Hence, we not only measured leg lengths and angles from the kinematic data but also estimated virtual leg lengths and virtual angles in accordance with the BSLIP model.

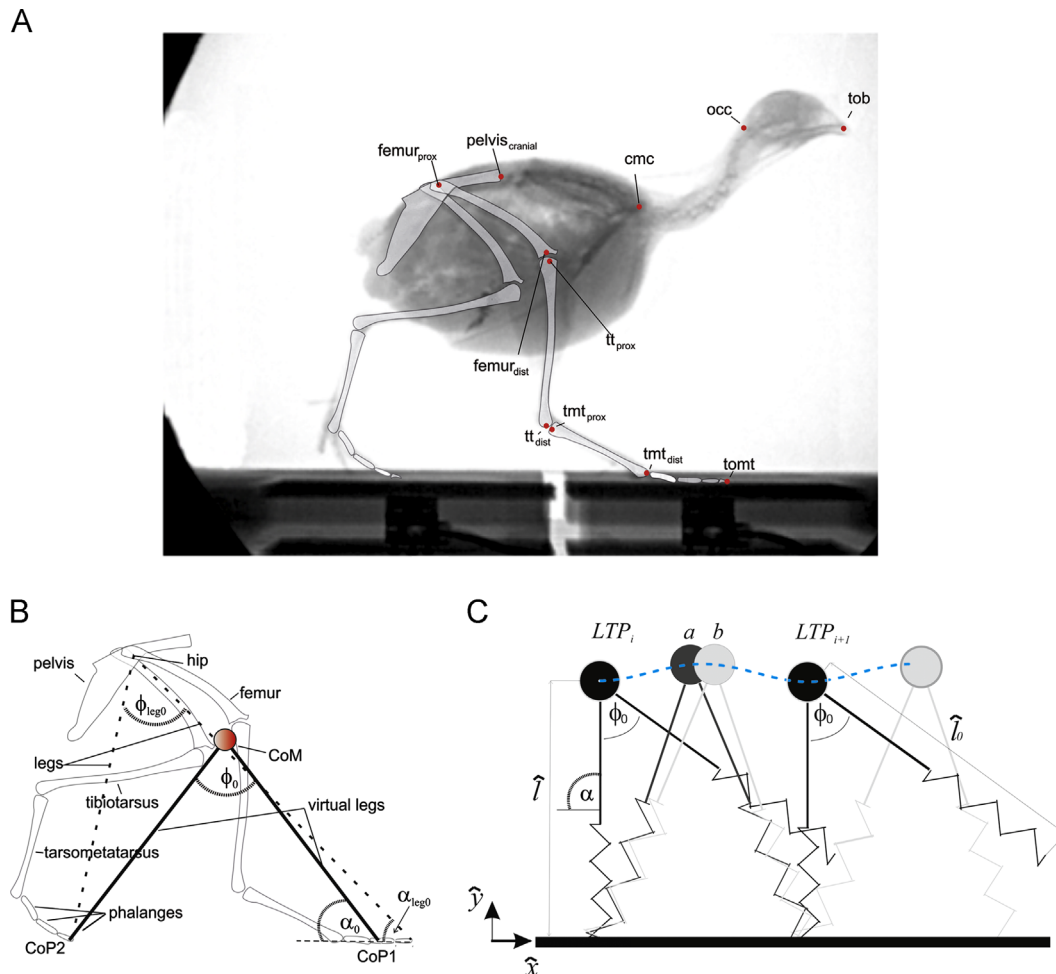


Fig. 1. (A) Latero-lateral x-ray projection of a quail traversing the two custom built force plates to obtain single limb kinetic data. Schematic drawing superimposed to x-ray image depicting all used landmarks to compute CoM kinematically. tob, tip of beak; occ, occiput; cmc, caudalmost cervical vertebrae; tomt, tip of middle toe. (B) Legs and virtual legs at touch-down (segments tomt1–hip–tomt2 and CoP1–CoM–CoP2). ϕ_{leg0} is the aperture angle between legs, ϕ_0 is the angle of attack between virtual legs, and α_0 is the angle of attack, and α_{leg0} is the orientation of the leg, all measured at touch-down. (C) Grounded running modeled with the bipedal spring loaded inverted pendulum (BSLIP) template. In the BSLIP, the body is represented by a point-mass (large dot) and mass-less leg springs of rest length \hat{l}_0 . Leg compression ψ is the difference of \hat{l}_0 and leg length \hat{l} at the lower turning point (LTP) of the CoM trajectory. Note that the leg's rest length \hat{l}_0 equals \hat{k} (see Section 2.2). Grounded running is characterized by a single and a double-support phase. Starting from LTP_i, the model progresses in single-support until the swing leg hits the ground (a) initiating the double support phase. With sufficient momentum, the forward progression continues until the hindmost stance leg reaches its resting length (take-off, b). From this instant, the model re-enters the single support phase until LTP_{i+1} is reached.

We estimated the position of the CoM by a combination of kinetic and kinematic measurements. We determined the CoM trajectory by double integration of the anterior-posterior and vertical accelerations (a_x ; a_y) obtained from the measured GRF divided by body mass. For the integration, four initial conditions (s_{0x} , s_{0y} , v_{0x} , v_{0y}) are required. CoM initial positions (s_{0x} , s_{0y}) were obtained from segment kinematic data (Fig. 1A) in combination with cadaveric information as described by Nyakatura et al. (2012), [see also Supplementary material]. As kinematic methods do not account for movement of appendages and viscera, kinematically determined CoM initial speeds (v_{0x} ; v_{0y}) are imprecise. Since a small error in v_{0x} results in a large position error (Daley et al., 2006), we optimized initial speeds by minimizing the sum of squared distances between the kinematically determined CoM trajectory and the force plate derived CoM trajectory as described in (Daley et al., 2006). This method allows for small discrepancies between force plate derived CoM trajectories and kinematic CoM trajectories, preventing their progressive divergence. Then, we computed the instantaneous virtual leg length as the distance between CoM and CoP.

As leg length in our model is symmetric related to touch-down (TD) and take-off (TO) events, we averaged related virtual leg lengths in order to determine the leg stiffness k from kinetic data. We computed k as $k = \text{GRF}_{\text{midstance}}/\Delta l$, where $\Delta l = (l_{\text{leg_TD}} + l_{\text{leg_TO}})/2 - l_{\text{leg_midstance}}$, and $l_0 = (l_{\text{leg_TD}} + l_{\text{leg_TO}})/2$. We used this stiffness to estimate the natural frequency $\omega_0 = \sqrt{k \cdot m^{-1}}$ and the dimensionless stiffness $\hat{k} = \hat{l}_0 = \omega_0^2 g^{-1} l_0$ (see Section 2.2). We measured the speed at minimum height ν to obtain $GR = \nu \omega_0/g$. We divided $\text{GRF}_{\text{midstance}}$ by body weight to determine leg compression $\psi = \text{GRF}_{\text{midstance}}/\text{BW}$ (for more information about dimensionless parameters see Section 2.2).

We determined the time course of the leg orientation (α_{leg}) and the virtual leg orientation (α) as the angle measured counter-clockwise between the ground and the segment hip joint–tips of the middle toes (tomt) and between the ground and the segment CoM–tomt, respectively (Fig. 1B). Moreover, we determined the time course of the aperture angle between legs (ϕ_{leg} ; tomt_{leg1}–hip joint–tomt_{leg2}) and virtual legs (ϕ ; CoP_{leg1}–CoM–tomt_{leg2}; Fig. 1B). Then, we determined the angle of attack of the virtual leg at touch-down (α_0) as the angle measured counter-clockwise between the ground and the segment CoM–CoP of the new stance leg, and the aperture angle between virtual legs ϕ_0 at touch-down by computing the angle between the CoPs of the stance legs and the CoM. Finally, we computed linear correlations and linear regression models between model-based experimental parameters using SPSS 18 (IBM, Armonk, NY, USA).

2.2. Dimensionless BSLIP model

In this study, we describe the gait dynamics of birds' grounded running with the BSLIP model. The BSLIP model consists of the body as a point mass m at the CoM and two massless, linear springs with a given stiffness k and rest length l_0 describing the action of the legs during stance. Each spring acts independently, and the swing phase is used to adjust the angle of attack related to the ground or the aperture angle related to the stance leg (see Fig. 1C). Motion is restricted to the sagittal plane, hence the equations of motion of the CoM are:

$$m\ddot{x} = -k(l_0 - l_1) \cos \alpha_1 - k(l_0 - l_2) \cos \alpha_2 \quad (1)$$

$$m\ddot{y} = -mg + k(l_0 - l_1) \sin \alpha_1 + k(l_0 - l_2) \sin \alpha_2, \quad (2)$$

where \ddot{x}, \ddot{y} are the accelerations and the positions of the CoM, m is the body mass, g is the gravitational acceleration, l_1 and l_2 are the instantaneous leg lengths during stance, and α_1 and α_2 are the corresponding orientations between the ground and each leg.

In the single-support phase (SSPh), only one leg exerts force and the last right-hand term in both equations is zero, whereas in the double-support phase (DSPh) both legs exert force and hence, all right-hand terms in both equations are nonzero. In a first step we replaced $\cos \alpha_i$ and $\sin \alpha_i$ by their correspondent cathetus-hypotenuse-ratios $(x - x_{\text{FPi}})/l_i$ (with x_{FPi} being the footpoints' x -coordinates and l_i the respective leg length) and y/l_i .

The use of templates (Bullimore and Donelan 2008; Full and Koditschek, 1999) for describing gaits permits the comparison of different species based on the template's parameters. To facilitate the comparison of species, we reformulated the system in a dimensionless way. Nondimensionalization of the template yields a minimum number of parameters. To distinguish dynamically different behavior with characteristic numbers such as dimensionless speed, the units should reflect basic system properties. Birds can locomote without aerial phases up to Froude numbers of 2 (Hancock et al., 2007), whereas Froude numbers in excess of 1 predict aerial phases. Hence the typically used time unit $\sqrt{l_0 \cdot g^{-1}}$ (e.g. Geyer et al., 2006), which is related to the Froude number, did not seem appropriate. The dynamics of human running are largely determined by SLIP quantities like stiffness of the spring and mass of the body (Maykranz et al., 2012). We assume that the same holds for bird grounded running. Therefore, we accounted for the natural frequency of the oscillator $\omega_0 = \sqrt{k \cdot m^{-1}}$ by choosing $T = \omega_0^{-1}$, $L = g \cdot \omega_0^{-2}$ and $M = m \cdot g \cdot \omega_0^{-2} \cdot l_0^{-1}$ as pertinent units for time, length, and mass. In consequence, dimensionless length, speed and acceleration (indicated by hat) relate to the dimensional quantities (here explicitly shown for \hat{x}) as $\hat{x} = L^{-1}x = \omega_0^2 g^{-1} x$, $\hat{x}' = T^1 L^{-1} \dot{x} = \omega_0 g^{-1} \dot{x}$ and $\hat{x}'' = T^2 L^{-1} \ddot{x} = g^{-1} \ddot{x}$, with prime denoting the derivative with respect to dimensionless time.

Substituting these expressions in (Eq. 1 and 2) resulted in the following dimensionless equations of motion for single ($a=1$) and double support phase ($a=2$):

$$\hat{x}'' = \sum_{i=1}^a \hat{x}_{\text{rel},i} \left(\frac{\hat{l}_0}{\hat{l}_i} - 1 \right) \quad (3)$$

$$\hat{y}'' = -1 + \sum_{i=1}^a \hat{y} \left(\frac{\hat{l}_0}{\hat{l}_i} - 1 \right) \quad (4)$$

where \hat{x}'', \hat{y}'' , \hat{x}, \hat{y} are the dimensionless accelerations and positions of the CoM, $\hat{x}_{\text{rel},i} = \hat{x} - \hat{x}_{\text{FPi}}$ are the relative \hat{x} -coordinates of the CoM with respect to the feet, $\hat{l}_i = \sqrt{(\hat{x}_{\text{rel},i})^2 + \hat{y}^2}$ are the stance legs' dimensionless lengths and \hat{l}_0 is their dimensionless rest length. Note that, by our choice of dimensionless units, the leg rest length $\hat{l}_0 = L^{-1}l_0 = \omega_0^2 g^{-1} l_0$ equals the dimensionless stiffness $\hat{k} = T^2 M^{-1} k = \omega_0^2 g^{-1} l_0$. Finally, the dimensionless leg compression is $\psi = \hat{l}_0 - \hat{l} = k(l_0 - l) m^{-1} g^{-1}$.

2.3. Simulations

2.3.1. Simulations with fixed aperture angle and with fixed angle of attack

In grounded running, as opposed to walking, the touch-down of the swing leg initiating the DSPh must occur when the mass moves upwards. Applying the fixed aperture angle ϕ_0 between legs, the touch-down of the swing leg occurs when $\hat{y} = \hat{l}_0 \sin(\alpha - \phi_0)$, where α is the instantaneous stance leg angle with respect to the ground measured clockwise. In contrast, using the fixed angle of attack α_0 , touch-down of the swing leg occurs when $\hat{y} = \hat{l}_0 \sin \alpha_0$. This behavior may be biologically motivated with an extending leg. The DSPh finishes when the hindmost leg reaches its slack length \hat{l}_0 and becomes the swing leg of the following step.

2.3.2. Stability analysis

To compare the stability of BSLIP grounded running using both, the fixed angle of attack and the fixed aperture angle, we performed a stability analysis using the Poincaré map e.g. Parker and Chua (1989). Then, for a rather intuitive assessment of model behavior to perturbations, we extended our analysis with the steps to fall method Seyfarth et al., 2002.

In cyclic locomotion, continuous evolution of the n -dimensional system state in time (here CoM state $(\dot{x}, \dot{y}, \dot{x}', \dot{y}')$) repeatedly intersects transverse $n-1$ -dimensional subspaces. We define such subspace for our system using the single support lower turning point (LTP) of the CoM trajectory ($\dot{y}' = 0$, inversion from negative to positive). The dimension of this subspace is further reduced by energy conservation. We select the horizontal speed \dot{x}' to be defined by the constant dimensionless system energy \hat{E} (see next paragraph; note that the conservative BSLIP model cannot abolish perturbations with respect to energy and hence, technically, only partial asymptotic stability can be achieved). Further, for stability only the relative distance of the CoM to the footpoint \hat{x}_{rel} is relevant. Then, the CoM state at LTP at step i is defined by $(\hat{x}_{rel}, \dot{y})_i$. Our Poincaré map \mathbf{P} discretely maps the state $(\hat{x}_{rel}, \dot{y})_i$ to $(\hat{x}_{rel}, \dot{y})_{i+1}$ defining a single step. We neglect two- or more-periodic solutions corresponding, for example, to limping gaits

or skipping. Fixed points in this map represent periodic solutions of the continuous time system and fulfill $(\hat{x}_{rel}, \dot{y})_i = (\hat{x}_{rel}, \dot{y})_{i+1}$.

The dimensional energy of the system at LTP is $E = mgy + (1/2)m\dot{x}^2 + ((k/2)(l_0 - l)^2)$. By substituting the dimensional variables y, \dot{x}, l_0 and l with their dimensionless counterparts, we obtained $\hat{E} = E(k/m^2g^2) = \dot{y} + (\dot{x}'^2/2) + ((\hat{l}_0 - \hat{l})/2)$, which, for given system state and \hat{E} , yields \dot{x}' . We call \dot{x}' the grounded running speed GR .

Based on our experimental data (see Section 2.1), we investigated the parameter space ranging from $1.5 \leq \hat{E} \leq 15$, $2 \leq k \leq 10$, and $45^\circ \leq \phi_0 \leq 80^\circ$ for periodic solutions. We determined \mathbf{P} by integrating Eqs. 3 and 4 numerically from LTP _{i} to LTP _{$i+1$} . The range of possible initial states is constrained by (I) vertical force greater than body weight (velocity inversion at LTP), i.e. vertical leg compression $\psi \cdot \sin \alpha$ is greater than 1, (II) kinetic energy greater than zero. We chose a grid of 80×80 from minimal to maximal possible initial states. Then, we used intersections of nullclines in \mathbf{P} (contour lines corresponding to zero change in the CoM states \hat{x}_{rel} and \dot{y}), respectively, as initial conditions for a subsequent fixed point iteration (Parker and Chua, 1989). Applying a two-dimensional Newton–Raphson algorithm in this iteration (Parker and Chua, 1989), we identified a fixed point when deviations $|\hat{x}_{rel,i+1} - \hat{x}_{rel,i}|$ and $|\dot{y}_{i+1} - \dot{y}_i|$ were less than 10^{-9} . We scanned the parameter

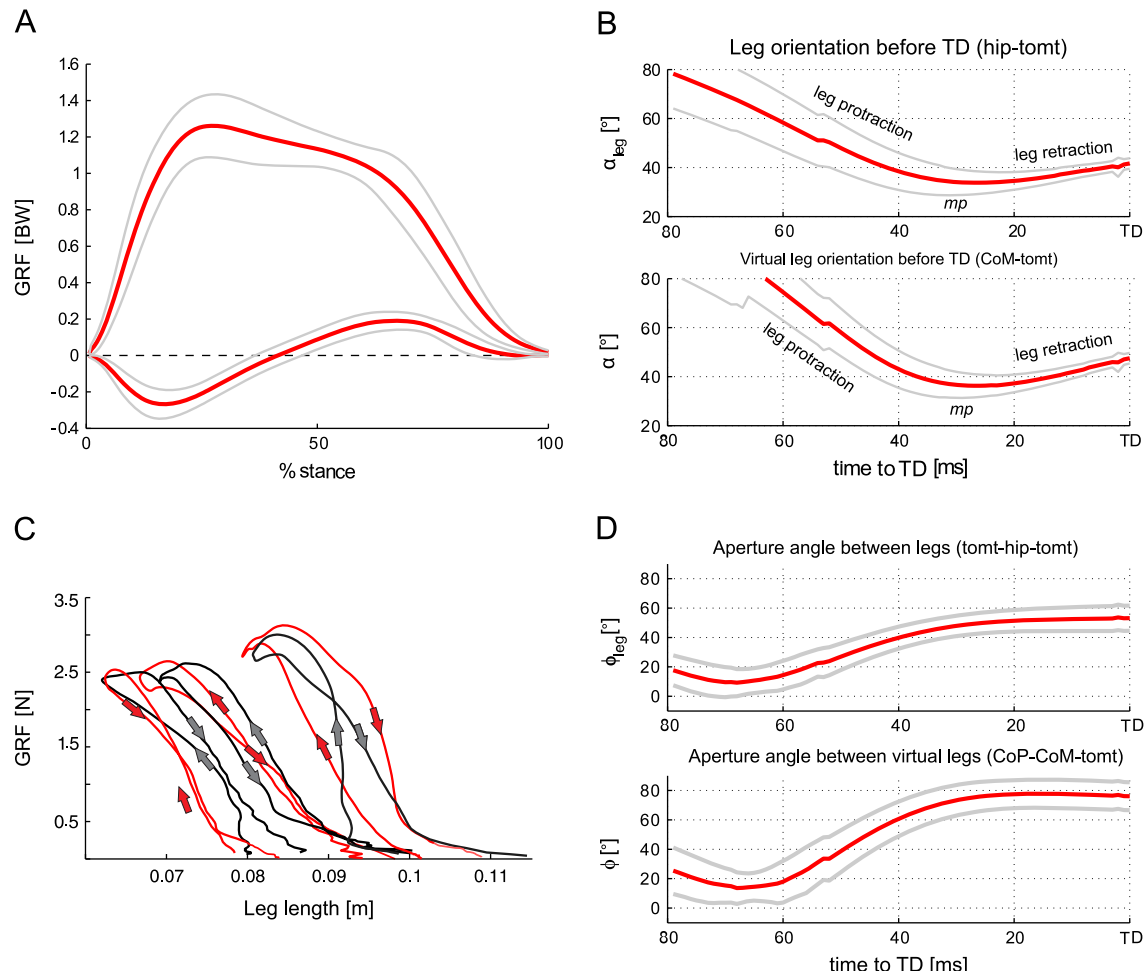


Fig. 2. (A) Vertical and anterior–posterior ground reaction forces related to stance duration during grounded running. Red bold curve: mean ($n=36$); grey curves represent ± 1 standard deviation (s.d.). (B) Leg orientation (top) and virtual leg orientation (bottom) in the last 80 ms before TD (sagittal plane projection). Orientation decreases as the leg is protracted until 20–30 ms before TD (maximum protraction *mp*). From this instant, it increases (leg is retracted) until TD. Red bold curve: mean ($n=18$); grey curves represent ± 1 s.d. (C) Force-displacement characteristics indicating spring-like behavior of the legs. Data of three different subjects, two steps (red and gray) each. (D) Aperture angle between legs (top) and aperture angle between virtual legs (bottom) in the last 80 ms before TD (sagittal plane projection). The aperture angle between legs is close to zero at midstance when legs are parallel. From this instant it increases as the swinging leg is rotated forward up to 20–30 ms before TD. From this point, the angle is kept constant until TD. Red bold curve: mean ($n=18$); grey curves represent ± 1 s.d. (For interpretation of the references to color in this figure legend, the reader is referred to the web version of this article.)

space systematically for fixed points taking a $24 \times 24 \times 24$ sample distributed equally in the three directions of the parameter space.

Next, for the fixed point search in a refined parameter space sample of $100 \times 100 \times 100$, we adopted a technique that took less computation time. Every successful fixed point search described in the preceding paragraph resulted in a single, symmetric fixed point, i.e. $\dot{x}_{rel} = 0$ for each fixed point, and leg compressions ψ at LTP remained within a lower range ($1.05 < \psi < 2$) of possible values bounded by conditions I) and II) (compare preceding paragraph). Instead of calculating the Poincaré map, we simply defined ten CoM initial conditions $(0, \dot{y}_i)$ for the fixed point iteration. According to the results obtained with the previous method, we chose them in a way that they concentrated in the range of the possible fixed point states. More specifically, let ub be the upper bound ($\hat{k} - 1.05$) and lb the lower bound of the possible \dot{y} -range. Then, we subsequently used $\dot{y}_i = ub - (ub - lb) \cdot \frac{1.3^{i-1}-1}{1.3^9-1}$, $i=1, \dots, 10$ for the fixed point iteration until success.

In the next step, we tested the periodic solutions for local stability of the conservative system. To obtain the linearized Poincaré map (**DP**) we applied perturbations of 10^{-5} to each state. Fixed points, and hence the corresponding continuous-time limit cycle, are locally stable if the eigenvalues λ_i of

$$DP = \begin{pmatrix} \frac{\partial \dot{x}_{rel,i+1}}{\partial x_{rel,i}} & \frac{\partial \dot{x}_{rel,i+1}}{\partial y_i} \\ \frac{\partial \dot{y}_{i+1}}{\partial x_{rel,i}} & \frac{\partial \dot{y}_{i+1}}{\partial y_i} \end{pmatrix} \quad (\text{also called Jacobian matrix})$$

unit circle, i.e. $|\lambda_i| < 1$ (Parker and Chua, 1989). The magnitude of the eigenvalues can be regarded a measure of stability.

Motivated by large differences found in the magnitude of the eigenvalues for the different leg alignment strategies (fixed aperture angle, fixed angle of attack), we assessed the effect of perturbations on the stability of the BSLIP model with the steps to fall method (Seyfarth et al., 2002). This method may give an estimate of how quickly the controller must react once the system is substantially driven away from its periodic locomotion mode (see (Seyfarth et al., 2002) for a motivation of this approach). We started simulations with fixed point parameters. Based on the observed maximal vertical foot ground clearance ($(\sin \alpha_{leg,TD} - \sin \alpha_{leg,mp})l_0 \approx 0.11 l_0$, where mp denotes maximum protraction, see Fig. 2B), we applied a vertical perturbation of 10% leg rest length. To keep the system energy constant, we chose step-up step-down and step-down step-up perturbations. We counted how many steps the BSLIP model could achieve after the perturbation. For practical reasons, we stopped the simulations after 50 steps. During aerial phases ($F_{leg} = 0$ for both legs) the fixed angle of attack or the fixed aperture policy was kept. In case of fixed aperture, both legs rotated with the same angular speed as those measured before TO. Quails rarely use aerial running during terrestrial locomotion even at high speeds (Gatesy and Biewener, 1991). Nevertheless, double contact phases are short for fast grounded running (about 40 ms). It seems reasonable to assume that if short aerial phases occur, the fixed aperture angle will be maintained. We implemented the simulation model in MATLAB/SIMULINK® (The MathWorks Inc., Natick, MA, USA). To integrate Eqs. 3 and 4 we applied a Runge–Kutta variable-step algorithm (ode45) with a relative and absolute integrator error tolerance of $1e-9$ and $1e-10$.

3. Results

3.1. Experimental data

Crossing our observation window (38×38 cm), quails usually accelerated or decelerated. From a total of 125 trials, eighteen steady grounded runs were obtained (speed range: $0.40 \text{ m/s} < v_x < 0.80 \text{ m/s}$).

The use of a fixed aperture angle (angle between legs) could be verified. If one follows the time course of both the leg (α_{leg}) and virtual leg orientation (α) (Fig. 2B), a leg retraction in the last 30 ms before TD can be observed. On the other hand, both, the aperture angle between legs ϕ_{leg} and the aperture angle between virtual legs ϕ increased as the swing leg was rotated forward up to 20–30 ms before TD (Fig. 2D). Notably, from this point, both angles were kept constant until TD.

The fixed aperture angle between virtual legs at TD (ϕ_0) varied between 55° and 73° , with a mean of $65.1^\circ \pm 5^\circ$ standard deviation (s.d.), and increased with grounded running speed GR ($r=0.832$; $p < 0.01$). Also, the angle between legs, \hat{k} and the leg compression increased significantly with GR ¹. In contrast, the angle of attack of the virtual leg showed no significant correlation with speed or with other variables (\hat{k}, ϕ_0, ψ). The mean-value of ϕ_0 at TD was $57.6^\circ \pm 3.4^\circ$ s.d.

The vertical component of the GRF showed a positively skewed flattened half-sine pattern, while anterior–posterior GRF approximated negative sine-waves (Fig. 2A). Peak-values of the vertical GRF increased with speed from 1.1 BW to 1.6 BW. Mean peak values measured for the anterior–posterior GRF oscillated between -0.25 BW and 0.2 BW (Fig. 2A). The time course of leg-length roughly followed a negative half-sine pattern. At take-off, leg-length was on average 7% longer than the length measured at touch-down (Fig. 2C). Besides this hysteresis, the force-length characteristic of the leg (Fig. 2C) supports a modeling approximation with a linear spring.

3.2. Simulations

Using the fixed aperture angle, periodic grounded running (Fig. 3A) covered 1/3 of the investigated $(\hat{k}, \phi_0, \hat{E})$ -space with a minimum system energy of 2.

Due to unique, symmetric ($\dot{x}_{rel} = 0$ at LTP) periodic solutions per parameter combination, we transformed the $(\hat{k}, \phi_0, \hat{E})$ -space into the (\hat{k}, ϕ_0, GR) -space and additionally included the leg compression ψ at LTP to completely characterize the system's point of operation (Fig. 4A). GR is higher than 8. Leg compressions ψ comprise the range of 1.05 to 1.71. The range $\psi < 1.6$ contains 97% of all periodic solutions. At constant values of ψ , when \hat{k} increases, ϕ_0 decreases (Fig. 4B). No changes in ϕ_0 , \hat{k} or ψ are necessary to achieve periodic grounded running for increasing speed (Fig. 4A).

The amount of leg compression ψ at the instant of the inversion of vertical speed defines the gait. If ψ is smaller than one (which means, that the force exerted is less than 1 BW), the vertical speed changes from positive (up) to negative (down) corresponding to the walking gait. If ψ is greater than 1, the vertical speed changes from negative to positive. If ψ is greater than 1.05 and smaller than 1.71, the gait is grounded running. Higher values of ψ correspond to aerial running.

Using the fixed aperture strategy, all periodic solutions are locally weakly unstable. Two separated spiral solution subdomains (complex eigenvalues, with a mean of their absolute values of 1.038 ± 0.025 s.d.; more than 84% of all periodic solutions) are connected in the middle by a rather narrow corridor of saddle points (mean of the eigenvalues 1.022 ± 0.028 std; Fig. 4C).

Using a purely mathematical fixed angle of attack strategy, i.e. the foot is allowed to “touch-down” when actually increasing its vertical position due to upwards movement of the CoM (Fig. 3B), the local stability of the solutions changes drastically. Most fixed points become strong unstable saddle points (97%; mean of the

¹ A complete list of correlations between model-based experimental parameters can be found in Table 1. Table 2 presents linear regression models of the significant correlations.

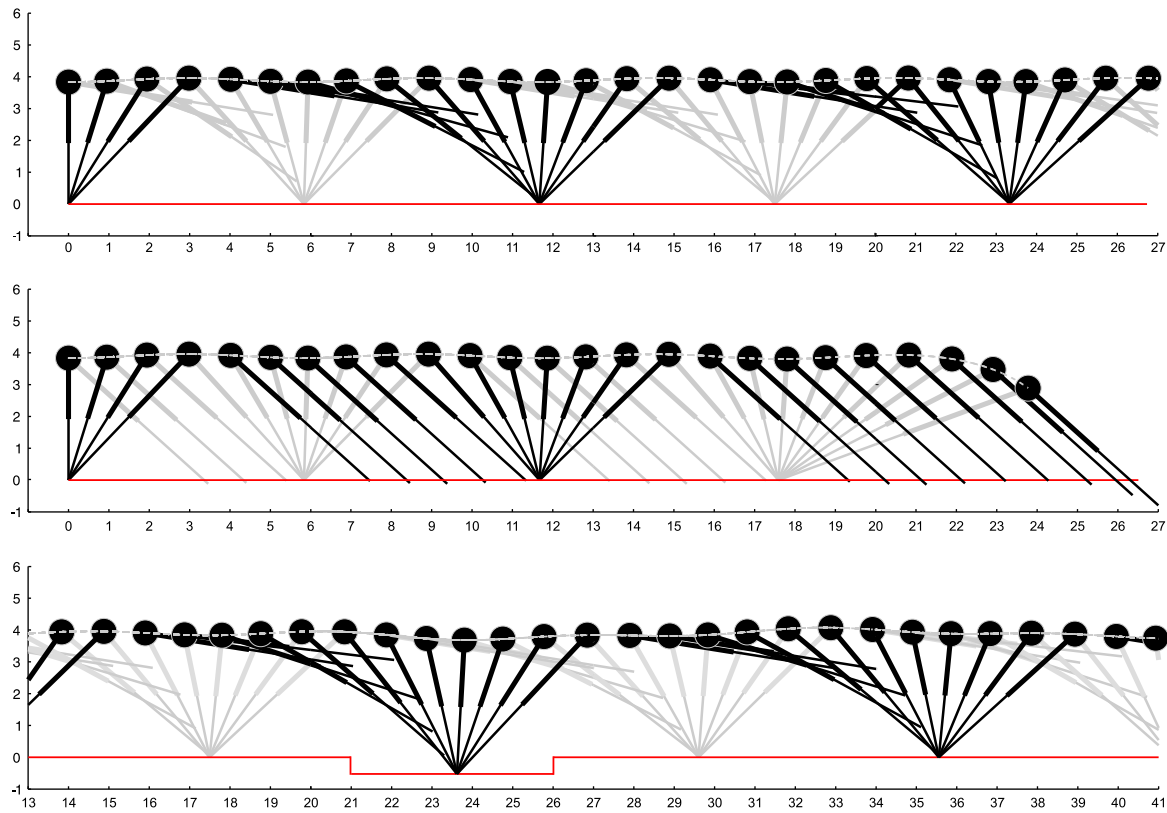


Fig. 3. Stick figure animations of grounded running simulations. Simulations use identical parameters. (A) Periodic locomotion obtained by using the fixed aperture angle strategy. Note the large leg compressions compared to rather small vertical excursions of the center of mass. (B) Simulation using a fixed angle of attack strategy. In a purely mathematical approach, the foot is allowed to touch-down while moving upwards crossing the surface level. Strong instability prevents the model from accomplishing further steps. (C) By using the fixed aperture angle strategy, the model can locomote more than 50 steps after a large perturbation of 10% of leg length without control.

eigenvalues 21.8 ± 18.4 s.d.), 2.5% become strong unstable spiral solutions (mean of the eigenvalues 11.2 ± 26.4 s.d.), and, surprisingly, 0.5% become stable fixed points (Fig. 4D).

Large perturbations did not pose a major problem for the BSLIP when using the fixed aperture angle (Fig. 3C). In 87% of the simulations the BSLIP reached 50 steps without falling, in 6% 25 to 49 steps, in 5% 15 to 25 steps, and in 2% 1 to 15 steps (Fig. 5A). Flight phases occurred in 52% of the simulations corresponding to higher \hat{k} and ψ values (Fig. 5B). In two fifth of those simulations the first flight phase occurred during the perturbation. Similar results were obtained for the step-up step-down perturbation. In contrast, using the fixed angle of attack, the step-up step-down perturbation cannot be coped with because the swing leg never reaches the touch-down condition. The same holds for 60% of step-down step-up simulations. Although the BSLIP can reach touch-down in the remaining simulations (using flight phases at higher \hat{k} and ψ values for step-up), the vast majority of those simulations reaches only two or three steps to fall. A marginal number (.05%) accomplishes more than 10 steps to fall.

4. Discussion

In the present work we analyzed quails' grounded running by experiments and by simulations. We present for the first time experimental evidence that quails fix the angle between legs before TD. Additionally, we show numerically that this leg alignment strategy in BSLIP grounded running improves local stability and tolerance to large perturbations compared to the fixed angle of attack strategy.

4.1. Fixed aperture angle vs. fixed angle of attack—Experiments

During the swing phase both, the maximum protraction angle with respect to ground and the swing time, are independent of speed in investigated bird species. This has been observed independent of whether or not the species are adapted to terrestrial locomotion (Gatesy and Biewener, 1991; Nyakatura et al., 2012; Verstappen et al., 2000; Fujita, 2004). As higher step length is required for higher speeds, the birds increase the rotation speed of their stance leg in order to lengthen their steps (Gatesy and Biewener, 1991; Verstappen et al., 2000; Fujita, 2004), which leads to increased aperture angles between legs (ϕ_{leg}).

In our study, at all observed speeds, the aperture angle changed only up to about 20–30 ms before TD and then remained constant until TD (Fig. 2B). Hence, the observed retraction of the swing leg (Fig. 2B) seems to be produced by a coupling to the rotation of the stance leg. The observed smaller standard deviation of the angle of attack versus the aperture angle (Fig. 2B and D) might at first glance suggest that quails control the angle of attack. However, the contraction of the periodic solution space (Fig. 4B and D) shows that the BSLIP model is less sensitive to ϕ_0 than to α_0 , which undermines such a conclusion. Consequently, the aperture angle strategy is more robust to errors in sensing and setting parameters. Also, it is not clear how animals should directly control the angle of the swing leg with respect to the ground, especially for birds that do not see their legs. In contrast, the aperture angle may be assessed by information from muscle spindles of few muscles in combination with an internal kinematic model of the leg. Furthermore, the enhanced space of periodic solutions allows the aperture angle to adapt to speed, leg stiffness, and leg compression whereas the angle of attack does not correlate with any of these variables (Table 1). Afferent signals from different sources within

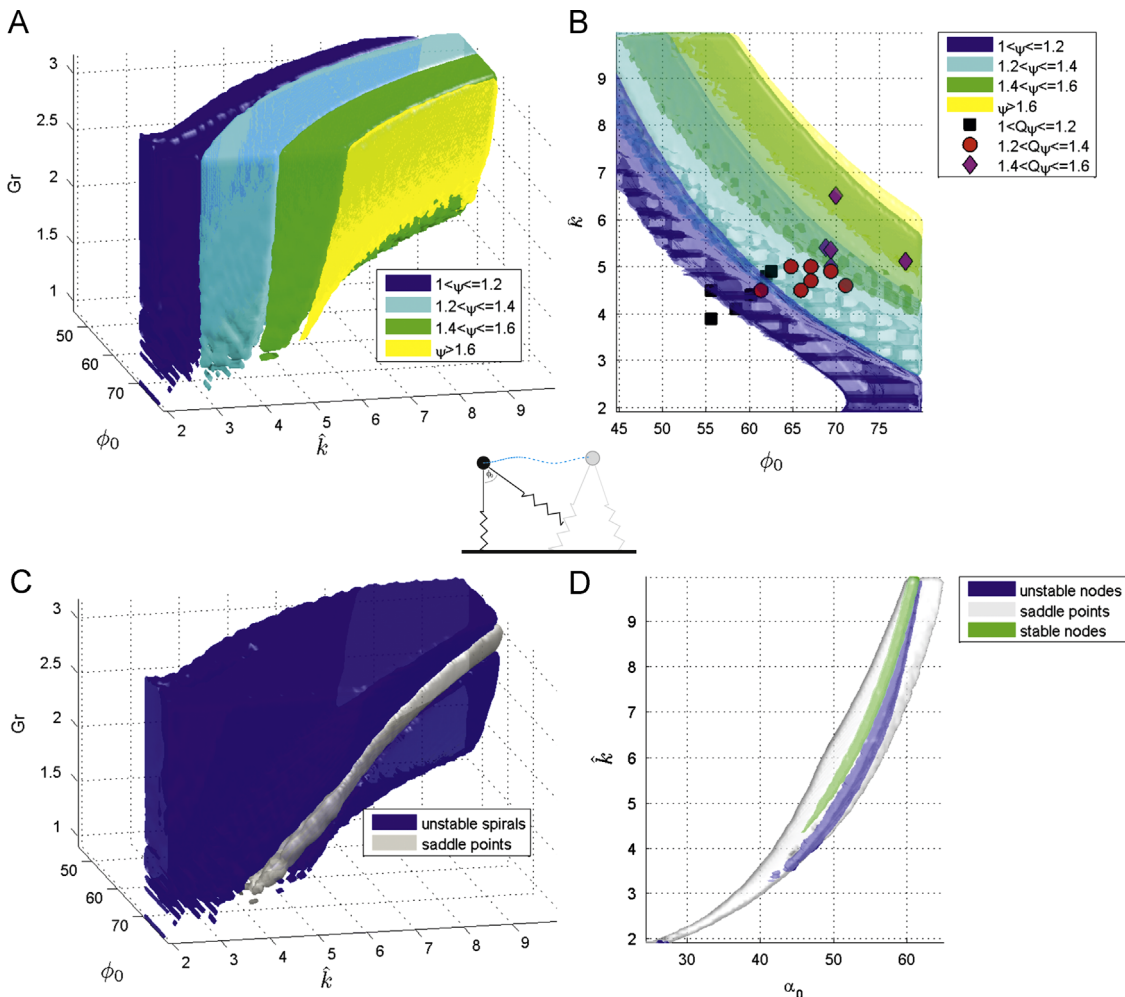


Fig. 4. Periodic solutions in grounded running. ((A), (B), (C)) The 3-D parameter domain corresponding to fixed points is simply connected and comprises one third of the investigated parameter space. To improve conceivability and to simplify comparison to experimental data, energy was replaced by the grounded running speed GR , thereby introducing some artifacts for low stiffness, high aperture angles and low Gr . (A) Leg compression ψ increases with \hat{k} and ϕ_0 . (B) Comparison of simulated periodic solutions and experimental data. Squares, circles, and diamonds represent model-based experimental parameters obtained from quails ($n=18$, see Section 2.3.4). Quails mainly employ parameters within section of BSLIP periodic solutions indicating relevance of the model. Other animals, running dynamically different to the quail, may use other parameter sections. (C) Local stability type of the periodic solutions using the fixed aperture strategy. Fixed points are characterized by two subdomains of weakly unstable spirals separated by a narrow subdomain of saddle points. (D) Local stability type of the periodic solutions using the fixed angle of attack strategy. The (\hat{k}, α_0) projection of the (k, α_0, \dot{E}) parameter space shows the typical J-shape known from BSLIP walking and running. A vast majority of the periodic solutions are strongly unstable. Marginally stable solutions comprise a thin sheet of 0.5% of the periodic solutions. Comparing (B) and (D), note the shrinkage of the area of periodic solutions (corresponding to a volume contraction by a factor of 6, see Supplementary material).

the legs can be used to adjust this adaption in dependence of speed, or environmental conditions.

A further effect of the swing leg policy applied by birds is improved ground speed matching of the leg tip, thereby reducing collisional energy loss. As stance leg rotation is coupled to swing leg rotation, retraction speed increases with increasing speed and, following, speed differences between the leg tip and the ground are smaller compared to fixed swing leg angle of attack with respect to the ground.

4.2. Fixed aperture angle vs. fixed angle of attack—Stability

Setting a fixed aperture angle or a constant angle of attack represent two different leg alignment strategies, and, therefore, affect the local stability of the periodic solution and also the response of the system to larger perturbations.

For the fixed aperture strategy, most of the periodic solutions are locally weakly unstable (Fig. 4C). However, the measure of local stability does not contain information about how quickly a controller would have to react to larger perturbations to prevent

falling. For the majority of simulations, the BSLIP achieves a minimum of 50 steps after large perturbations. The fixed aperture strategy leads to improved ground clearance of the leg tip in the swing phase. By its large compliance, the model is able to continue forward locomotion even in case of shallow angles of attack. Those results reveal one important advantage of running with compliant, crouched posture: no rash parameter changes may be imperative to cope with large perturbations.

Applying the fixed angle of attack as a leg alignment strategy, periodic solutions can be found only by allowance of touchdown in a purely mathematical way, namely when the foot of the swing leg moves upwards and meets the condition $\dot{y} = \dot{y}_0 \sin \alpha_0$. Though 0.5% of the periodic solutions are stable, the vast majority of them are strongly unstable and even perturbations within numerical errors lead to only three or four steps to falling (e.g. Fig. 3B). Stable solutions comprise a very narrow corridor, which exists only for relative high leg compressions ($\psi > 1.40$). This narrow corridor is surrounded by strongly unstable solutions. Further, simulations showed that leg alignment using a fixed angle of attack is geometrically not feasible to deal with large perturbations.

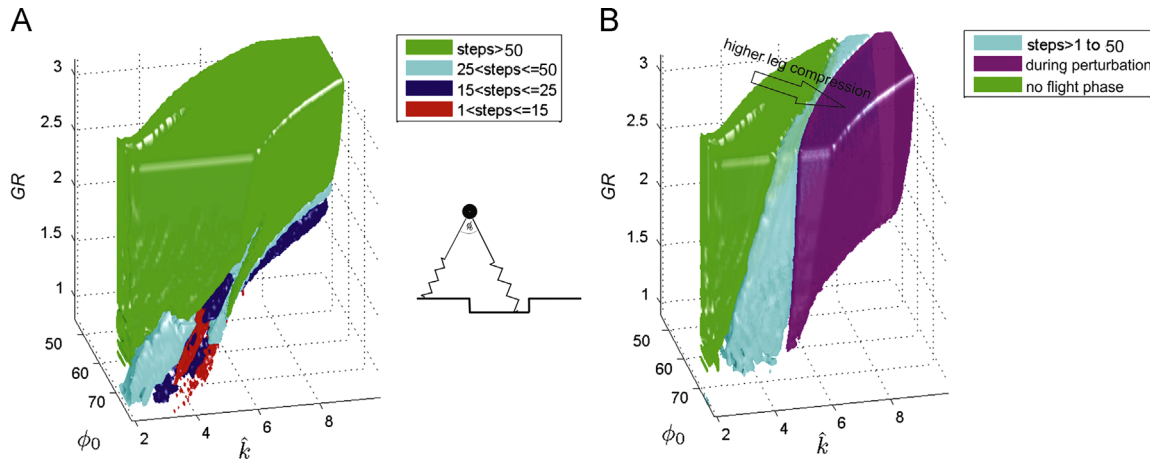


Fig. 5. System behavior after 10% leg length step-down, step-up perturbation using the fixed aperture angle. Step-up step-down perturbation of same magnitude leads to similar results (not shown). Simulations started with fixed point parameters and, for practical reasons, were stopped after 50 steps. The fixed angle of attack strategy leads to stumbling for the step-up step-down perturbations. For the step-down step-up perturbation only in 40% of cases the tip of the swing leg reached ground level, and in most cases, the model fell after one or two steps. (A) Steps to fall after perturbation. The color codes the number of steps reached. (B) Steps to first flight phase. Higher leg compressions lead to earlier aerial phase.

Table 1

Correlation between model-based experimental parameters. Significant correlation coefficients are bold (*: $p < 0.05$; **: $p < 0.01$). Correlations between α_0 , ϕ_{lego} , ϕ_0 , and ψ , $n = 18$. Correlations between GR and \hat{k} , $n = 36$. Mean values of GR or \hat{k} obtained from two consecutive steps were used for computing their correlations with α_0 , ϕ_{lego} , ϕ_0 , and ψ . Index 0 indicates the respective angles at touch down.

	α_0	ϕ_{lego}	ϕ_0	ψ	\hat{k}	GR
Angle of attack (α_0)	1	-.485	-.109	.05	.537	.0503
Aperture angle between legs (ϕ_{lego})	-.485	1	.751**	.827**	.319	.840**
Aperture angle between virtual legs (ϕ_0)	-.109	.751**	1	.782**	.592*	.832**
Leg_compression (ψ)	-.05	.827**	.782**	1	.331	.747**
Dimensionless stiffness (\hat{k})	.537	.319	.592*	.331	1	.657**
Dimensionless speed (GR)	.503	.840**	.832**	.747**	.657**	1

Table 2
Linear regression models between model-based experimental parameters.

Linear model	Regression's equation	r^2	p-value
\hat{k} –GR	$\hat{k} = 1.21\text{Gr} + 3.24$	0.432	< 0.001
ψ –GR	$\psi = 0.27\text{Gr} + 0.883$	0.558	< 0.001
ϕ_0 –GR	$\phi_0 = 10.12\text{Gr} + 49.2 [^\circ]$	0.692	< 0.001
ϕ_{lego} –GR	$\phi_{lego} = 15.46\text{Gr} + 38.4 [^\circ]$	0.706	< 0.001
ϕ_0 – \hat{k}	$\phi_0 = 3.6\hat{k} + 46 [^\circ]$	0.35	0.026
ϕ_0 – ψ	$\phi_0 = 24.6\psi + 32.7 [^\circ]$	0.612	0.001
ϕ_{lego} – ψ	$\phi_{lego} = 37.32\psi + 13 [^\circ]$	0.685	< 0.001
ϕ_0 – ϕ_{lego}	$\phi_0 = 0.5\phi_{lego} + 33.8 [^\circ]$	0.564	0.001

For number of samples used to compute each regression see caption Table 1.

The step-up step-down perturbation of 10% leg rest length, which may be common in the environment, especially of small birds, cannot be coped with since the tip of the swing leg does not reach ground level. The situation improves only little for step-down step-up due to strong local instability of the BSLIP model using the fixed angle of attack.

4.3. Model predictions vs. experimental data

Our simulations predict periodic grounded running at leg compressions ranging from 1.05 to 1.71 BW. Notably, quails did not show leg compressions lower than 1.1 and higher than 1.6 BW during grounded running, a range containing 97% of the BSLIP periodic solutions. In addition, quails mostly use parameters not leading to aerial phases during the large perturbation in simulations (Figs. 4 and 5B). This agrees with the notion that birds try to

maintain continuous ground contact, and thus maneuverability, during uneven locomotion (Gatesy and Biewener, 1991; Daley and Usherwood, 2010).

In contrast to our simulations, where grounded running speed GR can be increased without any changes in stiffness, aperture angle, or leg compression (Fig. 4A), the experimental results show a positive correlation between GR and these parameters. This *prima facie* conflicting result may be explained by neglected leg mass and inertia in the BSLIP model. As speed increases in simulations, constant values of \hat{k} , ϕ_0 , and ψ lead to prolonged double support phases while the legs' contact times remain constant. This requires unrealistically short swing phases, which may not be achievable with real legs with inertia (remember that swing time in birds remains constant independent of speed). Simulations using a more complex model with leg mass may explain observed correlations.

The numerical searches yielded purely symmetric periodic solutions within the parameter range, i.e. both the shape of the GRF and the leg length are symmetric related to the TD and TO events. This finding may be somewhat surprising. The BSLIP model has asymmetric solutions for walking (Geyer et al., 2006), while the SLIP model can produce only symmetric solutions for running (Schwind, 1999). One may therefore expect, that the double contact phase allows asymmetric solutions. But in the case of grounded running (having double support phases), no asymmetric solutions were found.

Our experimental observations on quails show, however, that (i) the shape of the GRF resembles a positively skewed flattened half-sine pattern (Fig. 2A), (ii) the leg lengthens from touch-down to take-off (mean ca. 7%) and (iii) the stiffness changes during the

stance phase during grounded running (Fig. 2C). Leg lengthening has also been observed during human walking and running (Lipfert, 2010). Small birds walk and run with a more crouched posture than humans, which gives them an even greater capacity for leg lengthening (Gatesy and Biewener, 1991). Furthermore, leg lengthening coupled to the process of retraction during the swing phase may be a strategy to prevent birds from falling (Daley and Usherwood, 2010; Daley et al., 2007). Variations in rest length l_0 or stiffness k in the dimensional BSLIP model can potentially explain the skewed time course of the GRF. These features are not included in our model, and further investigations are needed to understand their functional importance.

4.4. The usefulness of grounded running

Contrary to the concept of impulsive running (Srinivasan and Ruina, 2006), the legs of small birds operate particularly compliant (Muir et al., 1996, this study). Besides the fact that muscle properties enforce compliance, the cost of driving a compliant leg can be reduced by introducing spring-like tissues (Rode et al., 2009; Srinivasan, 2010). For example, the elastic recoil was measured to be up to 60% of the work performed per step in running wild turkeys (Roberts et al., 1997). Grounded running represents a gait in which the storage mechanism may be exploited at speeds in which aerial phases (running) are absent (Nudds et al., 2011; Rubenston et al., 2004).

As grounded running is accompanied by low stiffness ((McMahon et al., 1987), own results), it seems to be especially suited to small animals which favor crouched and therefore compliant positions ((McMahon, 1985), own results). In many larger animals, swing leg inertia and decrease of effective mechanical advantage prevent such positions during gait, and, accordingly, high stiffness and more extended legs can be observed and grounded running is avoided. It should be noted that, following these arguments, grounded trotting, ambling or even grounded galloping (canter without aerial phases) may be a typical feature of small animals' locomotion.

The crouched (grounded+crouched) gait offers the advantage of long step lengths and contact times, enhancing maneuverability while improving the distribution of ground reaction forces. The latter reduces peak reaction forces compared to gaits which feature greater limb stiffness. While energy storage and the reduction in peak force may help to reduce the cost of locomotion, the decrease in the effective mechanical advantage of the musculature may cancel out this effect (Gatesy and Biewener, 1991; McMahon et al., 1987; Biewener 1989).

It should be noted that the presence or lack of stable solutions for grounded running does not necessarily translate to the stability or instability of grounded running in the animal. Additional feed-forward leg placement control or muscle pre-activation could change the stability of the system as shown in previous experiments (Daley et al., 2006, 2007; Biewener and Daley, 2007; Birn-Jeffery and Daley, 2012) and simulation studies (Blum, et al.; Ernst, et al.).

Our results may motivate engineers of compliant robots to explore the possibilities of grounded running. Grounded running with compliant legs enables high locomotion speed with low peak loading forces exceeding slightly body weight. This implies that vertical oscillations of the center of mass are low, which simplifies visual sensing. Furthermore, fixed aperture angle could represent an easily implementable low-level control option that improves ground speed matching by automatically adapting swing leg retraction velocity to forward speed. This reduces impact and resulting high frequency oscillations, which can produce both structure damage and/or deviations from reference trajectories. Resulting weak instability may easily be corrected for by slow (e.g. stride-to-stride) high-level control. Suitable design parameters

and points of operation can be directly inferred from the dimensionless formulation and the corresponding diagrams (Fig. 4A, B).

Acknowledgments

We thank our project partners John Nyakatura and Martin Fischer for providing the animals, the x-ray laboratory, and helping us with the high speed x-ray analysis. John Nyakatura also provided helpful critique on early drafts of the manuscript and helped with the design of Fig. 1. We also thank Michael Ernst for stimulating helpful discussions on self-stability. This research was supported by the DFG grants BI 236/22-1 (to R. Blickhan) and FI 410/15-1 (to M.S. Fischer).

Appendix A. Supporting information

Supplementary data associated with this article can be found in the online version at <http://dx.doi.org/10.1016/j.jtbi.2013.06.031>.

References

- Ahn, A.N., Furrow, E., Biewener, A.A., 2004. Walking and running in the red-legged running frog, *Kassina maculata*. *J. Exp. Biol.* 207, 399–410, <http://dx.doi.org/10.1242/jeb.00761>.
- Biewener, A.A., 1989. Scaling body support in mammals: limb posture and muscle mechanics. *Science* 245, 45–48.
- Biewener, A.A., Daley, M.A., 2007. Unsteady locomotion: integrating muscle function with whole body dynamics and neuromuscular control. *J. Exp. Biol.* 210, 2949–2960, <http://dx.doi.org/10.1242/jeb.005801>.
- Birn-Jeffery, A.V., Daley, M.A., 2012. Birds achieve high robustness in uneven terrain through active control of landing conditions. *J. Exp. Biol.* 215, 2117–2127, <http://dx.doi.org/10.1242/jeb.065557>.
- Blickhan, R., 1989. The spring-mass model for running and hopping. *J. Biomech.* 22, 1217–1227, [http://dx.doi.org/10.1016/0021-9290\(89\)90224-8](http://dx.doi.org/10.1016/0021-9290(89)90224-8).
- Blickhan, R., Seyfarth, A., Geyer, H., Grimmer, S., Wagner, H., Gunther, M., 2007. Intelligence by mechanics. *Philos. Transact. A Math. Phys. Eng. Sci.* 365, 199–220, <http://dx.doi.org/10.1088/rsta.2006.1911>.
- Blum, Y., Birn-Jeffery, A., Daley, M.A., Seyfarth, A., Does a crouched leg posture enhance running stability and robustness? *J. Theor. Biol.* 281, 97–106.
- Bullimore, S.R., Donelan, J.M., 2008. Criteria for dynamic similarity in bouncing gaits. *J. Theor. Biol.* 250, 339–348, <http://dx.doi.org/10.1016/j.jtbi.2007.09.038>.
- Cavagna, G.A., 1975. Force platforms as ergometers. *J. Appl. Physiol.* 39 (1), 174–179.
- Cavagna, G.A., Thys, H., Zamboni, A., 1976. The sources of external work in level walking and running. *J. Physiol.* 262, 639–657.
- Clark, J., Alexander, R.M., 1975. Mechanics of running by quail (*Coturnix*). *J. Zool.* 176, 87–113, <http://dx.doi.org/10.1111/j.1469-7998.1975.tb03189.x>.
- Daley, M.A., Usherwood, J.R., 2010. Two explanations for the compliant running paradox: reduced work of bouncing viscera and increased stability in uneven terrain. *Biol. Lett.* 6, 418–421.
- Daley, M.A., Usherwood, J.R., Felix, G., Biewener, A.A., 2006. Running over rough terrain: guinea fowl maintain dynamic stability despite a large unexpected change in substrate height. *J. Exp. Biol.* 209, 171–187, <http://dx.doi.org/10.1242/jeb.01986>.
- Daley, M.A., Felix, G., Biewener, A.A., 2007. Running stability is enhanced by a proximo-distal gradient in joint neuromechanical control. *J. Exp. Biol.* 210, 383–394, <http://dx.doi.org/10.1242/jeb.02668>.
- Dietz, V., 1996. Interaction between central programs and afferent input in the control of posture and locomotion. *J. Biomech.* 29, 841–844.
- Ernst, M., Geyer, H., Blickhan, R., Extension and customization of self-stability control in compliant legged systems. *Bioinspiration Biomimetics*. 7, 046002.
- Fujita, M., 2004. Kinematic parameters of the walking of herons, ground-feeders, and waterfowl. *Comp. Biochem. Physiol. A: Mol. Integr. Physiol.* 139 (1), 117–124.
- Full, R.J., Koditschek, D.E., 1999. Templates and anchors: neuromechanical hypotheses of legged locomotion on land. *J. Exp. Biol.* 202, 3325–3332.
- Gatesy, S.M., Biewener, A.A., 1991. Bipedal locomotion: effects of speed, size and limb posture in birds and humans. *J. Zool.* 224, 127–147.
- Gatesy, S.M., Middleton, K.M., 1997. Bipedalism, flight, and the evolution of Theropod locomotor diversity. *J. Vert. Paleontol.* 17, 308–329.
- Geyer, H., Seyfarth, A., Blickhan, R., 2006. Compliant leg behaviour explains basic dynamics of walking and running. *Proc. R. Soc. London, Ser. B* 273, 2861–2867, <http://dx.doi.org/10.1098/rspb.2006.3637>.
- Hancock, J.A., Stevens, N.A., Biknevicius, A.R., 2007. Whole-body mechanics and kinematics of terrestrial locomotion in the elegant-crested Tinamou. *Eudromia elegans*. *Ibis* 149, 605–614.

- Heglund, N.C., Cavagna, G.A., Taylor, C.R., 1982. Energetics and mechanics of terrestrial locomotion. III. Energy changes of the centre of mass as a function of speed and body size in birds and mammals. *J. Exp. Biol.* 97, 41–56.
- Lipfert, S.W., 2010. Kinematic and Dynamic Similarities between Walking and Running. Verlag Dr Kovac, Hamburg.
- Maykranz, D., Grimmer, S., Seyfarth, A., accepted. A work-loop method for characterizing sagittal plane movements. *J. Appl. Biomech.*
- McMahon, T.A., 1985. The role of compliance in mammalian running gaits. *J. Exp. Biol.* 115, 263–282.
- McMahon, T.A., Valiant, G., Frederick, E.C., 1987. Groucho running. *J. Appl. Physiol.* 62, 2326–2337.
- Minetti, A.E., Ardigo, L.P., Saibene, F., 1994. The transition between walking and running in humans: metabolic and mechanical aspects at different gradients. *Acta Physiol. Scand.* 150, 315–323.
- Muir, G.D., Gosline, J.M., Steeves, J.D., 1996. Ontogeny of bipedal locomotion: walking and running in the chick. *J. Physiol.* 493 (Pt 2), 589–601.
- Nudds, R.L., Folkow, L.P., Lees, J.J., Tickle, P.G., Stokkan, K.A., Codd, J.R., 2011. Evidence for energy savings from aerial running in the Svalbard rock ptarmigan (*Lagopus muta hyperborea*). *Proc. R. Soc. London, Ser. B* 278, 2654–2661, <http://dx.doi.org/10.1098/rspb.2010.2742>.
- Nyakatura, J.A., Andrade, E., Grimm, N., Weise, H., Fischer, M.S., 2012. Kinematics and center of mass mechanics during terrestrial locomotion in Northern Lapwings (*Vanellus vanellus*, Charadriiformes). *J. Exp. Zool. A Ecol. Genet. Physiol.* 317, 580–594, <http://dx.doi.org/10.1002/jez.1750>.
- Parker, T., Chua, L., 1989. Practical Numerical Algorithms for Chaotic Systems. Springer, New York.
- Pearson, K.G., 1995. Proprioceptive regulation of locomotion. *Curr. Opin. Neurobiol.* 5 (6), 786–791.
- Roberts, T.J., Marsh, R.L., Weyand, P.G., Taylor, C.R., 1997. Muscular force in running turkeys: the economy of minimizing work. *Science* 275, 1113–1115.
- Rode, C., Siebert, T., Blickhan, R., 2009. Titin-induced force enhancement and force depression: a ‘sticky-spring’ mechanism in muscle contractions? *J. Theor. Biol.* 259, 350–360, <http://dx.doi.org/10.1016/j.jtbi.2009.03.015>.
- Rubenson, J., Heljams, D.B., Lloyd, D.G., Fournier, P.A., 2004. Gait selection in the ostrich: mechanical and metabolic characteristics of walking and running with and without an aerial phase. *Proc. R. Soc. London, Ser. B* 271, 1091–1099, <http://dx.doi.org/10.1098/rspb.2004.2702>.
- Rummel, J., Blum, Y., Seyfarth, A., 2009. From Walking to Running. Autonome Mobile Systeme 2009. Springer, pp. 89–96.
- Saibene, F., Minetti, A., 2003. Biomechanical and physiological aspects of legged locomotion in humans. *Eur. J. Appl. Physiol.* 88, 297–316, <http://dx.doi.org/10.1007/s00421-002-0654-9>.
- Schwind, W.J., Spring Loaded Inverted Pendulum Running: A Plant Model. Ph.D. Thesis. University of Michigan: Ann Arbor, MI, USA, 1999.
- Seyfarth, A., Geyer, H., Gunther, M., Blickhan, R., 2002. A movement criterion for running. *J. Biomech.* 35, 649–655, [http://dx.doi.org/10.1016/S0021-9290\(01\)00245-7](http://dx.doi.org/10.1016/S0021-9290(01)00245-7).
- Seyfarth, A., Geyer, H., Herr, H., 2003. Swing-leg retraction: a simple control model for stable running. *J. Exp. Biol.* 206, 2547–2555.
- Srinivasan, M., 2010. Fifteen observations on the structure of energy-minimizing gaits in many simple biped models. *J. R. Soc. Interface.* 8, 74–98, <http://dx.doi.org/10.1098/rsif.2009.0544>.
- Srinivasan, M., Ruina, A., 2006. Computer optimization of a minimal biped model discovers walking and running. *Nature* 439, 72–75.
- Verstappen, M., Aerts, P., Van Damme, R., 2000. Terrestrial locomotion in the black-billed magpie: kinematic analysis of walking, running and out-of-phase hopping. *J. Exp. Biol.* 203, 2159–2170.